Journal of Power Sources 477 (2020) 228567

Contents lists available at ScienceDirect

Journal of Power Sources

journal homepage: www.elsevier.com/locate/jpowsour

Operando investigation of the solid electrolyte interphase mechanical and transport properties formed from vinylene carbonate and fluoroethylene carbonate

Paul G. Kitz [a,b], Matthew J. Lacey [c,b], Petr Novák [a], Erik J. Berg [a,b,*]

[a] Electrochemistry Laboratory, Paul Scherrer Institute, CH-5232, Villigen, PSI, Switzerland
[b] Department of Chemistry, Ångström Laboratory, Uppsala University, Box 538, SE-751 21, Uppsala, Sweden
[c] Scania CV AB, SE-151 87, Södertälje, Sweden

HIGHLIGHTS

- The SEI mechanical and transport properties are measured by combined EIS & EQCM-D.
- VC and FEC reduce SEI thickness but only VC results in effective anode passivation.
- VC and FEC increase the SEI shear storage modulus on carbon.
- The interphase transport properties are influenced significantly by both additives.

ARTICLE INFO

Keywords:
Li-ion battery
SEI
Electrolyte additives
Electrochemical impedance spectroscopy
Electrochemical quartz crystal microbalance

ABSTRACT

The electrolyte additives vinylene carbonate (VC) and fluoroethylene carbonate (FEC) are well known for increasing the lifetime of a Li-ion battery cell by supporting the formation of an effective solid electrolyte interphase (SEI) at the anode. In this study combined simultaneous electrochemical impedance spectroscopy (EIS) and *operando* electrochemical quartz crystal microbalance with dissipation monitoring (EQCM-D) are employed together with *in situ* gas analysis (OEMS) to study the influence of VC and FEC on the passivation process and the interphase properties at carbon-based anodes. In small quantities both additives reduce the initial interphase mass loading by 30–50%, but only VC also effectively prevents continuous side reactions and improves anode passivation significantly. VC and FEC are both reduced at potentials above 1 V vs. Li^+/Li in the first cycle and change the SEI composition which causes an increase of the SEI shear storage modulus by over one order of magnitude in both cases. As a consequence, the ion diffusion coefficient and conductivity in the interphase is also significantly affected. While small quantities of VC in the initial electrolyte increase the SEI conductivity, FEC decomposition products hinder charge transport through the SEI and thus increase overall anode impedance significantly.

The maximum effective energy that is reversibly stored in a Li-ion battery cell generally decreases over its lifetime. Various aging mechanisms are responsible for this phenomenon. In the case of graphite anodes, which are used in most of today's Li-ion cells, the formation of a protective solid electrolyte interphase (SEI) at the electrode-electrolyte interface plays a key role in minimizing side reactions and thus enabling long battery cycle life [1]. The SEI inhibits the continuous decomposition of electrolyte at the carbonaceous anode, which is operating well below the cathodic stability limit of the carbonate based electrolyte.

It is generally acknowledged that the reduction of the electrolyte co-solvent ethylene carbonate (EC) during the initial formation cycles of the battery cell is critical for the development of this passivating interphase. However, the decomposition mechanism of EC is still under debate: While many studies show that the reduction of EC results in the formation of lithium ethylene dicarbonate (LEDC), recent results by Wang et al. suggest that lithium ethylene mono-carbonate (LEMC) is instead the main SEI forming decomposition product of this process [2,

* Corresponding author. Department of Chemistry, Ångström Laboratory, Uppsala University, Box 538, SE-751 21, Uppsala, Sweden.
E-mail address: erik.berg@kemi.uu.se (E.J. Berg).

https://doi.org/10.1016/j.jpowsour.2020.228567
Received 6 April 2020; Received in revised form 31 May 2020; Accepted 25 June 2020
Available online 18 August 2020

3]. To further improve the specific SEI properties in commercial battery cells (e.g. resistance, thickness, mechanical/thermal stability …) sacrificial additives are typically mixed into the electrolyte [4]. Vinylene carbonate (VC) and fluoroethylene carbonate (FEC) are popular additives used to enhance the SEI quality (Fig. 1) [5,6]. Both feature a relatively low LUMO level and are therefore reduced before EC at the anode-electrolyte interface during the first charge process. Most studies have found that small amounts of VC decrease SEI thickness, improve cell capacity retention, and increase the temperature stability of the interphase [7–11]. However, when coupled with a high-voltage cathode material, large amounts of VC can have a detrimental effect on cell impedance since the additive is oxidized above 4.3 V vs. Li^+/Li [12,13]. This is less of an issue for the fluorinated derivative FEC which features improved electrochemical stability at high potentials and has shown to stabilize the electrolyte in contact with high voltage cathodes [13–15]. FEC furthermore stabilizes the interphase on alloying type anode materials, such as silicon, which undergo large volume expansion during lithiation. It has also shown to improve the SEI properties on carbonaceous anodes [16–18].

By employing FTIR, XPS, NMR, OEMS, and other techniques, researchers have identified polymeric species (often denoted poly(vinylene carbonate), i.e., poly(VC)), Li_2CO_3, and CO_2 as the main VC reduction products [8–10,19,20]. The precise VC decomposition mechanism remains unclear, however. It is considered likely that the additive decomposes via an electrochemically triggered radical polymerization mechanism to form CO_2 gas and a cross-linked polymeric product which precipitates at the anode-electrolyte interface [8,9,19]. The Li_2CO_3 salt frequently detected alongside the organic VC decomposition products could originate from the reaction of CO_2 with hydroxide ions present in the electrolyte [21], or also from the direct reduction of either CO_2 [20,22] or poly(VC) [23] in contact with lithiated carbon.

Similarly to the case of VC, the anode-electrolyte interphase in cells with FEC appears to contain significant amounts of both inorganic Li_2CO_3 and polymeric species often denoted poly(FEC) [10,16]. However, in the presence of FEC, LiF salt is detected as another main SEI component [6,20,24]. Due to the similar reduction products formed by both additives, it is likely that the decomposition pathway of the FEC molecule in Li-ion cells is more similar to VC than to the structurally related co-solvent EC (Fig. 1). Based on these observations many different FEC reduction mechanisms have been proposed in literature [6,16,19,24–26]. Michan et al. studied FEC decomposition via chemical lithium naphthalenide reduction, for example [19]. The authors detected trace quantities of VC as an intermediate reaction product and therefore proposed that FEC is reduced via a one electron step to form LiF, H_2, and VC. However, computational modeling [26] and FEC radiolysis [25] suggest that LiF, CO_2, and a vinoxyl-radical, rather than VC, are the main reaction intermediates of FEC decomposition in Li-ion cells. In any case, the organic intermediate product will react further and produce CO_2, Li_2CO_3, and polymeric compounds (e.g. poly(FEC)) at the anode interface.

While the beneficial effect of VC and FEC on Li-ion battery cell performance is well documented, comparatively little is known about the influence of both additives on the SEI properties. Since VC and FEC reaction products change the interphase composition, it is expected that the additives also influence the SEI mechanical and transport properties. These factors are related to the SEI structural integrity and the electrode impedance and are of significant interest to the research community. Therefore, combined *operando* electrochemical quartz crystal microbalance with dissipation monitoring (EQCM-D) with simultaneous *in situ* electrochemical impedance spectroscopy (EIS) is employed in this study to directly measure and compare changes of the SEI properties on graphite anodes induced by VC and FEC in standard $LiPF_6$ based battery electrolyte. Online electrochemical mass spectroscopy (OEMS) and EQCM-D are furthermore utilized to compare the anode passivation process and quality during the initial formation cycles in the presence of EC, EC + VC, and EC + FEC.

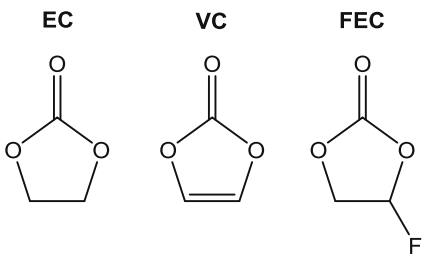

Fig. 1. Structural formula of the electrolyte co-solvent ethylene carbonate (EC) and the common electrolyte additives vinylene carbonate (VC) and fluoroethylene carbonate (FEC).

1. Experimental

1.1. Electrode and electrolyte preparation

Carbon (C) based QCM-sensors are prepared by coating commercial 5 MHz Au type sensors (Q-Sense, Biolin Scientific AB, Sweden) with first a 50 nm thick Cu adhesion film and then a 50 nm thick C active material layer by sputter deposition at room temperature. The resulting non-porous smooth surface C model electrodes with an active surface area of roughly 1.13 cm^2 have been characterized in a previous work [21]. LFP counter electrodes (CEs) are prepared by coating a slurry containing 80 wt% $LiFePO_4$ (LFP, Clariant AG, Switzerland), 10 wt% Super C65 carbon black (SC65, Imerys, Switzerland), and 10 wt% polyvinylidene fluoride (PVdF, Kynar HSV 900, France) dispersed in NMP (N-Methyl-2-pyrrolidone, Sigma-Aldrich, Switzerland) on an Al current collector foil with 500 μm wet thickness. Porous C based working electrodes (WE) are prepared similarly by coating a Cu current collector mesh (Dexmet Corporation, USA) with a mixture of 80 wt% SC65 and 20 wt% PVdF dispersed in NMP. The wet electrode sheets are dried at 80 °C under vacuum overnight. Afterwards, circular electrodes are punched out (Ø12 mm for EQCM-D and Ø18 mm for OEMS measurements), dried again at 120 °C under vacuum for >12 h, and are then introduced directly into an argon filled glovebox (O_2/H_2O < 0.1 ppm).

LP47 electrolyte consisting of 1 M $LiPF_6$ salt dissolved in a mixture of ethylene carbonate (EC) and diethylene carbonate (DEC, ratio 30:70 wt %) is used as the blank electrolyte in this study (BASF SE, Germany, H_2O content < 10 ppm as determined by Karl-Fischer titration). Different amounts of VC (Sigma-Aldrich, Switzerland) and FEC (BASF SE, Germany) are added to this solution in order to investigate their effect on the SEI formation mechanism. In commercial Li-ion battery cells, the concentration of electrolyte additives is typically quite low due to the high cost of these species and to prevent unwanted side effects during cycling [11–13]. In order to facilitate comparable results in research cells it is advantageous to use not the same electrolyte concentrations but rather similar ratios of overall additive amount to electrode surface area (flooding factor) as discussed in previous publications [12,16,17,21]. The electrolyte additive concentrations in this work are therefore adjusted (0.1 wt% for EIS/EQCM-D and 0.4 wt% for OEMS) and correspond to ~3.5 wt% additive used in a typical commercial electrolyte according to Pritzl et al. [12] and Burns et al. [11].

1.2. Measurements and data analysis

The experimental setups used for combined EIS/EQCM-D and for OEMS, respectively, are described in detail elsewhere [27,28]. In both cells the C based anodes are cycled versus a LFP CE between 3.0 V and 0.25 V vs. Li^+/Li with 0.1 mV s^{-1} cyclic voltammetry (CV) scan rate. LFP is used as a CE active material for all measurements since it operates around 3.45 V vs. Li^+/Li and therefore within the expected thermodynamic stability window of the carbonate-based electrolyte. However, for

easy comparison all electrochemical potentials in this study are referenced to the redox potential of metallic lithium and not LFP. During OEMS the gas evolution from the carbon black SC65 model anode is recorded every 15 min by a mass spectrometer. The EIS/EQCM-D cell is operated in four electrode configuration (see supporting information Fig. S1): A porous SC65 anode and a C coated QCM sensor are short-circuited and cycled together versus the CE while the QCM-sensor resonance frequency and dissipation changes are continuously recorded on multiple harmonic overtone orders. An additional Li-gold alloy micro reference electrode is implemented in the system to facilitate EIS measurements. During cycling the EIS spectrum of the C coated QCM-sensor is recorded every 250 mV. Detailed information on the measuring setup and procedure can be found elsewhere [27]. The time invariance of the EIS spectra has been validated by the Kramers-Kronig transformation using the Lin-KK tool (see Fig. S2) [29].

The QCM-sensor resonance frequency and dissipation changes are fitted with an acoustic multilayered viscoelastic Voigt model using a MATLAB script, as discussed in detail in previous publications [21,27]. Note that the SEI thickness and its viscoelastic properties are calculated in pure LP47, LP47 + VC, and LP47 + FEC by assuming an average SEI density of $\rho_{SEI} = 1.3$ g cm^{-3} on the C coated sensor. This value has been measured by Kwon et al. in $LiClO_4$/EC + EMC electrolyte using EQCM and ellipsometry [30]. While the SEI is expected to feature a similar density in pure $LiPF_6$/EC + DEC, it is possible that ρ_{SEI} is higher if VC or FEC is added to the electrolyte since increased amounts of inorganic salts (Li_2CO_3, LiF) are precipitating on the electrode surface in this case. Therefore, the corresponding SEI thickness and its mechanical property values reported in this work might be slightly overestimated. However, this possible error is too small to significantly affect any conclusions made in this work (see Fig. S3 and Fig. S4).

2. Results and discussion

2.1. Interphase formation mechanism in the presence of VC or FEC

Fig. 2 presents the C QCM-sensor anode current, the interphase mass change, and the SEI and electrolyte property changes captured by EQCM-D during the first three CV cycles in LP47, LP47 + VC, and LP47 + FEC electrolyte. The corresponding gas evolution rates from a porous SC65 carbon black anode during interphase formation are presented in Fig. 3. The data set using blank LP47 electrolyte has been discussed in detail in a previous publication and is shown here for comparison [21]. No significant reactions appear to occur in the first cycle at high potentials > 2.5 V in any of the three tested systems. The anode mass remains constant and no gas evolution is detected from the cell in this potential regime.

However, around 2 V vs. Li$^+$/Li trace water impurities start to be reduced which initiates the subsequent autocatalytic hydrolysis of EC and causes the evolution of CO_2 gas and the precipitation of poly ethylene glycol (PEG) type species at the carbon anode interface [21,31].

$$H_2O + e^- \rightarrow OH^- + \tfrac{1}{2} H_2 \quad (1)$$

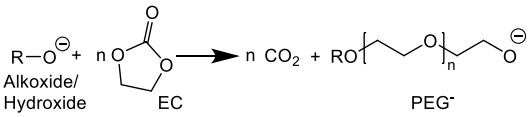

(2)

The process is marked by high electrode mpe-values > 100 g mol^{-1} (mpe: mass change per mole of electrons transferred), since EC is decomposed in a chemical reaction following the reduction of small amounts of H_2O, and results in an early sensor mass increase by ~2 μg cm^{-2} in both VC and FEC containing electrolyte (Fig. 2 b). Surprisingly, this process appears to produce a measurable interphase on the anode at a ~400 mV more positive potential in the EQCM-D cell filled with LP47 + FEC electrolyte compared to LP47 + VC. This discrepancy is not

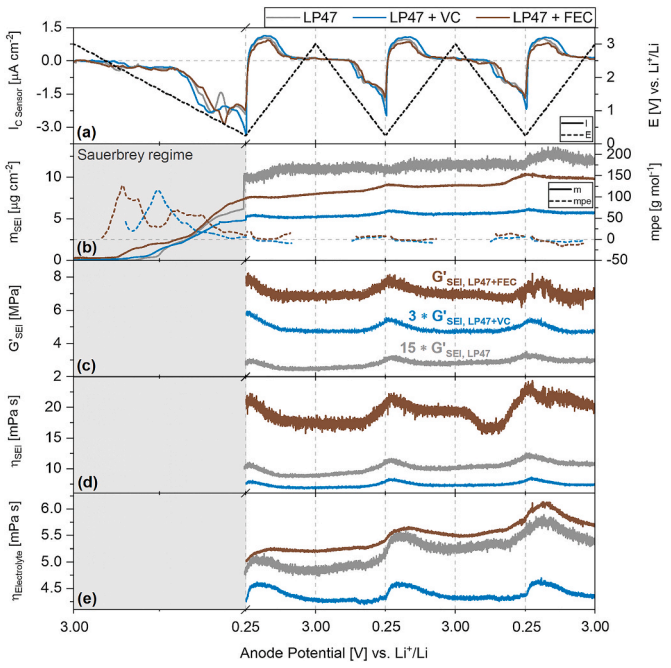

Fig. 2. Interphase formation on a C coated QCM-sensor cycled between 3.00 and 0.25 V vs. Li$^+$/Li with 0.1 mV s^{-1} CV scan rate in LP47, LP47 + 0.1 wt% VC, or LP47 + 0.1 wt% FEC electrolyte (blank LP47 data set from previous publication [21]). Figures (a)–(b) present the C coated QCM-sensor potential, current, mpe-value, and the interphase mass change during cycling. Figures (c), (d), and (e) show the SEI shear storage modulus (G'_{SEI}), the SEI viscosity (η_{SEI}), and the electrolyte viscosity ($\eta_{electrolyte}$) in vicinity of the QCM-sensor as calculated from the QCM-sensor resonance frequency and dissipation data.

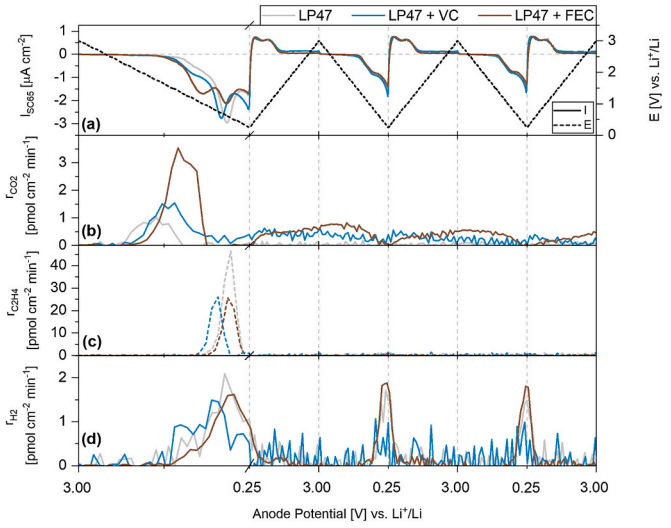

Fig. 3. Gas evolution from a carbon black SC65 porous anode cycled between 3.0 and 0.25 V vs. Li$^+$/Li with 0.1 mV s^{-1} CV scan rate in LP47, LP47 + 0.4 wt% VC, or LP47 + 0.4 wt% FEC electrolyte (OEMS experiments).

observed by OEMS (Fig. 3) and might be caused by different residual water concentrations in the cells. For example, a slightly higher water content in a cell will produce more hydroxide ions at early stages of cycling. This will accelerate the subsequent autocatalytic EC decomposition cycle significantly and therefore cause much earlier detection of this process by EQCM-D.

Below 1.6 V the early formed interphase on C impedes further water reduction and CO_2 evolution rates are decreasing in both pure LP47 and VC containing electrolyte (Fig. 3 b). The subsequent reduction of VC is

difficult to pinpoint due to the low concentration of the additive in the electrolyte and the autocatalytic radical-driven VC decomposition cycle likely initiated already by low reduction currents [8,9,19,20,32]. However, both the small mpe plateau at ~40 g mol^{-1} visible between 1.3 and 1.1 V vs. Li^+/Li (Fig. 2 b) and the at the same time higher CO_2 evolution rate in LP47 + VC (Fig. 3 b) compared to the additive free system indicate that VC is reduced in this potential regime. A similar onset potential for VC reduction on C was also found by Jeong et al. using *in situ* AFM [33]. The measured anode mpe value at this point is relatively low compared to the expected value for an electrochemically triggered polymerization of the additive, since this process overlaps with the simultaneous intercalation of Li into the C active material and the reduction of water, as discussed below.

In LP47 + FEC electrolyte significant amounts of CO_2 continue to evolve <1.5 V which results in a three times higher CO_2 gas amount generated in the first cycle compared to the cell with no additive (Fig. 3 b). Similar observations have previously been made in literature and can be clearly traced to the reduction of FEC [16,34]. The resulting interphase formation causes a broad plateau in the anode mpe value around 56 g mol^{-1} between 1.45 V–0.95 V. Surprisingly, FEC does not appear to increase the H_2 evolution rate (Fig. 3 d) as previously reported by Jung et al. [16]. It is possible however that the FEC concentration in this study is so low (0.1 wt%), that the additional H_2 evolution originating from the additive is below the detection limit of the OEMS setup.

Below 0.9 V the anode mpe-value and the CO_2 gas evolution rates in both LP47 + VC and LP47 + FEC have decreased significantly which indicates that both electrolyte additives are no longer reduced in this potential regime. The resulting anode-electrolyte interphase suppresses the subsequent reduction of EC as evidenced by the decrease of ethylene gas evolution rates by over 40% in both cases (reaction 3, Fig. 3 c). Interestingly, the EC reduction current peak and the corresponding C_2H_4 evolution appear at roughly 100 mV higher electrode potentials in VC containing electrolyte compared to pure LP47 or LP47 + FEC.

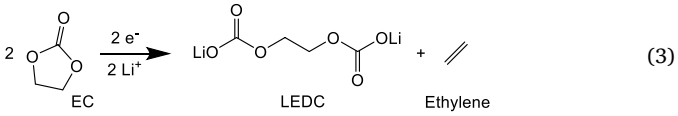

(3)

The hydrogen gas evolution rate increases below 1.5 V vs. Li^+/Li in all tested electrolytes in the first cycle (Fig. 3 d) due to the reduction of water as previously determined by combining OEMS with isotope labeled electrolyte (reaction 1) [21]. The subsequent autocatalytic decomposition of EC causes the formation of both CO_2 and soluble polymeric compounds according to reaction 2 which increases the electrolyte viscosity continuously during cycling (Fig. 2 e). While the addition of FEC does not appear to significantly alter this process, VC suppresses hydrogen gas generation in the 2nd and 3rd cycle (Fig. 3 d). This indicates that the SEI formed by both the reduction of VC and EC effectively prevents the continuous reduction of water at low electrochemical potentials. This could explain why the electrolyte viscosity in VC containing electrolyte remains 12% lower after the 1st cycle as compared to the additive free system and also why $\eta_{electrolyte}$ continues to increase at a much lower rate in the 2nd and 3rd cycle if VC is present in the system (Fig. 3 e, discussed in more detail below). Nevertheless, the ongoing evolution of CO_2 shown in Fig. 3 (b) indicates that EC hydrolysis is slowly progressing also in the VC system.

After the initial polarization to low potentials the SEI mass stabilizes in all cells (Fig. 3 b). The thin SEI formed in VC containing electrolyte improves anode passivation significantly which results in a three times lower rate of sensor mass increase during later cycles compared to the additive free system. In contrast, the anode passivation appears to be relatively poor in LP47 + FEC electrolyte which causes an ongoing increase of SEI mass and electrolyte viscosity during cycling. Besides the continuous hydrolysis of the electrolyte co-solvent EC it is possible that the anode passivation has not been completed after the first cycle in this case which could cause the reduction of FEC also in later cycles and might explain the stepwise QCM-sensor mass increase detected below 1.1 V vs. Li^+/Li in Fig. 2 b. It is important to note that the CO_2 evolution rate drops and does not increases in this potential regime, since the gas might be scavenged by hydro-/alkoxide ions and/or is directly reduced on the anode surface [20,21]. Furthermore FEC is known to slowly decompose over time in $LiPF_6$ based electrolytes [35,36]. Hydrogen fluoride generated by the reaction of the salt with traces of water impurities [37] might trigger a ring-opening and subsequent polymerization of the additive FEC. Corresponding solid and soluble fluorinated polymeric compounds have been detected by Xu et al. via NMR [35] and could result in the continuous increase of both SEI mass and electrolyte viscosity in FEC containing cells detected in this study by *operando* EQCM-D.

2.2. Interphase & electrolyte mechanical properties

VC and FEC have a significant impact on the SEI composition and its properties. After one reduction cycle the SEI in LP47 + VC features a mass of ~5.3 μg cm^{-2} which amounts to a ~41 nm thick interphase assuming an average SEI density of 1.3 g cm^{-3}. In LP47 + FEC the generated interphase is slightly thicker at ~7.5 μg cm^{-2} and ~58 nm, respectively. The addition of 0.1 wt% additive to the electrolyte therefore reduces the interphase mass in the case of FEC by 30% and for VC by 50% compared to the blank electrolyte [21]. These EQCM-D results are in accordance with previous observations by *in situ* AFM [33,38] and might suggest at first glance good anode passivation in both additive systems. However, while the SEI generated in LP47 + VC is relatively stable after the first CV cycle is completed, the interphase mass in LP47 + FEC is continuously increasing (Fig. 2 b). Moreover, the electrolyte remains overall less viscous in the cell containing VC compared to FEC which indicates that less soluble organic decomposition products are produced in this case. Based on these observations it is evident that the electrolyte additive VC offers far better passivation of the C anode as compared to both FEC and the blank electrolyte, which explains the improved electrochemical performance of graphite anodes in VC containing electrolytes as reported in the literature [13]. It is important to note that this is not necessarily the case for other types of electrodes. In particular alloying materials such as silicon, which undergo large volume expansion during lithiation and delithiation and therefore suffer from interphase cracking, can show better performance in electrolytes containing FEC compared to VC [39]. Whether the electrolyte additives have an impact on the mechanical SEI properties and might therefore cause these trends is discussed next.

VC reduction leads to the precipitation of Li_2CO_3, poly(VC), and possibly other polymeric and/or inorganic species on the C electrode surface [8–10,19]. The resulting interphase is much more rigid than the SEI formed in electrolyte with no additive present, as evident from the ~10 times higher SEI shear storage modulus presented in Fig. 2 (c). In FEC containing electrolyte a significant amount of rigid LiF salt is precipitating at the electrode surface additionally which increases the average SEI G′ modulus even further ($G'_{SEI,LP47} \approx 0.2$ MPa, $G'_{SEI,LP47+VC} \approx 1.6$ MPa, $G'_{SEI,LP47+FEC} \approx 6.9$ MPa). In their recent work Yoon et al. also observed a significant increase of the SEI rigidity on a Li metal substrate in the presence of FEC using a membrane bulge test which agrees with these *operando* EQCM-D results [40]. Yang et al. furthermore reported relatively similar SEI G′ modulus values in the low MPa range by EQCM-D on tin anodes in contact with an FEC containing electrolyte during early stages of cycling [41]. However, it is important to note that the authors used a roughly 100 times higher FEC concentration compared to this work, which might explain the much thicker and much more viscous electrode-electrolyte interphase encountered in their study.

The SEI viscosity on C anodes calculated in this work is presented in Fig. 2 (d). In general, η_{SEI} is not affected as significantly as G'_{SEI} by the electrolyte additives which could indicate similar interphase solvent penetration in all three cells. The increased amount of LiF salt in the SEI

does however lead to a roughly twice as viscous interphase in the case of FEC compared to both VC and the blank electrolyte ($\eta_{SEI,LP47} = 9$ mPa s, $\eta_{SEI,LP47+VC} = 7$ mPa s, $\eta_{SEI,LP47+FEC} = 17$ mPa s) [21]. It is important to point out that the actual SEI viscoelastic parameters might be slightly lower than the values calculated in this study due to a possible underestimation of interphase density during EQCM-D modelling. However, as shown in Fig. S3 and Fig. S4 this potential error is relatively small and does not change any trends discussed in this work.

As mentioned, the electrolyte viscosity remains the lowest in the cell containing LP47 + VC, likely due to the successful suppression of H_2O reduction (Fig. 2 e). FEC on the other hand increases $\eta_{electrolyte}$ compared to blank LP47, possibly due to the chemical reaction of the additive with HF impurities and the subsequent formation of soluble polymeric compounds [35].

The viscoelastic SEI parameters and the electrolyte viscosity in VC or FEC containing electrolyte change dynamically with electrochemical anode potential as already observed previously for the blank electrolyte (Fig. 3 c, d, e) [21]. These fluctuations are a result of the electrochemical and chemical processes, such as reversible Li-intercalation, water reduction, and/or EC hydrolysis, which occur at the anode and in the bulk electrolyte even after the formation of the passivating SEI. The underlying mechanisms are described in more detail elsewhere [21,27].

2.3. Anode and interphase electrochemical properties

The anode and SEI electrochemical properties at the C coated QCM-sensor cycled either in blank LP47, LP47 + 0.1% VC, or LP47 + 0.1% FEC electrolyte are studied next by impedance spectroscopy. Between 3 and 2 V vs. Li^+/Li the EIS spectrum features a mostly capacitive behavior similar to a delithiated graphite as typical for an electrode under blocking condition (Fig. 4 a) [42]. This indicates that no significant charge transfer reaction is occurring at the electrode interface in this potential regime and that the electrochemical behavior is instead dominated by the electrical double layer. However, the corresponding EIS spectra are not vertical, as would be expected from an ideal capacitor, but instead slightly tilted to the right. Reversible adsorption processes of charged species and/or electrode surface inhomogeneities might cause this non-ideal behavior [43]. The phase shift is the same in all three tested electrolytes ($CPE_p = 0.8$, Fig. 4 a) which suggests that this non-ideal behavior is an inherent feature of the SEI-free interface between the C sensor and $LiPF_6$ based electrolyte. This is the case for all impedance spectra recorded >1.5 V at the C anode with the exception of the first cycle around 2 V vs. Li^+/Li, likely due to partially reversible water reduction occurring on the SEI-free electrode in this potential regime, as discussed above.

Between 2 and 1 V vs. Li^+/Li the EIS spectrum transitions from a blocking electrode to an anode with reversible Li intercalation occurring at its interface (Fig. 4 b), as expected from the current profile in Fig. 2 a. The electrode impedance in this potential regime appears to be significantly higher in the first cycle compared to the subsequent cycles. This trend is particularly evident in the VC containing electrolyte in which the absolute anode impedance decreases by one order of magnitude between the first and second CV cycle at 1.25 V. The interphase formed <1 V in the first cycle might aid Li intercalation into the C anode and therefore cause this behavior e.g. by lowering the energy required for stripping the solvation shell off the Li-ions. It could be furthermore

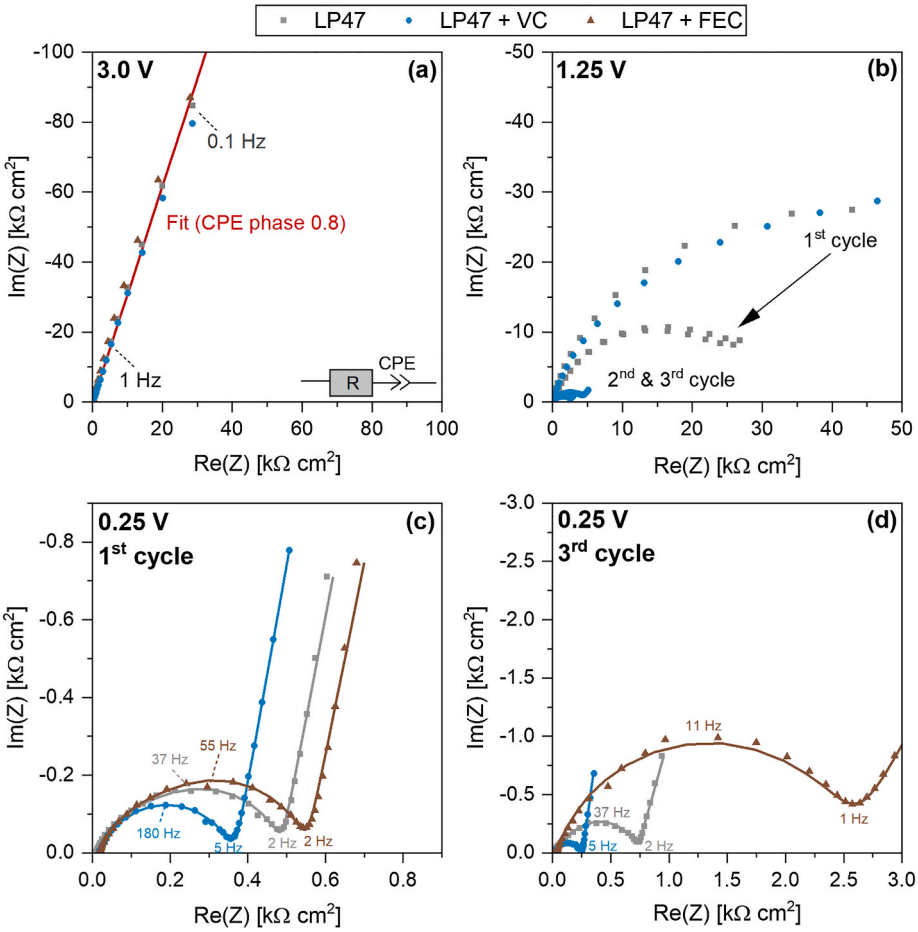

Fig. 4. EIS spectra of the C sensor anode in contact with pure LP47, LP47 + 0.1 wt% VC, and LP47 + 0.1 wt% FEC electrolytes at (a) 3.0 V, (b) 1.25 V, and (c) & (d) 0.25 V vs. Li^+/Li. The data for LP47 + FEC at 1.25 V is shown in Fig. S5. The data points are measured values while the lines represent corresponding equivalent circuit fits. The spectra at 0.25 V are fitted with the model in Fig. 5. The corresponding Bode plots for (c) and (d) are presented in Fig. S6.

imaginable that the reduced charge transfer resistance results from irreversible structure changes in the C electrode occurring in the first cycle. However, the latter is not detected by EQCM-D and therefore rather unlikely.

Fig. 4 (c) and (d) present the EIS spectra of the C coated QCM-sensor at 0.25 V vs. Li^+/Li in the first and third CV cycle. Below 1 V the charge transfer reaction initiated by reversible Li insertion into the C bulk material produces a single depressed semicircle in the high to mid frequency region. From the Bode plot it is evident that at least two time constants define this electrode behavior (Fig. S6). During cycling the anode impedance in blank LP47 is generally growing, particularly in the mid to low frequency region, most likely because both the SEI and the electrolyte become more resistive. The latter is caused by the increasing electrolyte viscosity during cycling as seen in Fig. 2 (e). The electrolyte additive VC appears to lower and FEC to increase the C model anode impedance during Li insertion according to Fig. 4 (c) and (d). These differences continue to grow during cycling which is surprising since most reports in literature suggest that the anode impedance increases and not decreases if VC is added to the electrolyte [12,44]. However, Burns et al. also observed a slight drop of the anode resistance if relatively low amounts of VC are used [11]. Since VC decomposes by an electrochemically triggered radical polymerization process it is likely that the SEI becomes thicker the more additive is present in the cell which results in an increase of the anode impedance with growing VC concentration [11,12]. The relatively high amount of additive used in most studies in literature could therefore explain why VC is generally believed to increase and not decrease the C anode impedance during cycling. It is furthermore important to note that VC oxidizes at cathodes operating above ~4.3 V vs. Li^+/Li which also influences cell resistance significantly [11,12].

The sputtered C anode EIS spectra captured during reversible Li intercalation in Fig. 4 (c) and (d) are relatively similar to the EIS response of graphite anodes at low potentials [45]. In literature the data is typically analyzed by fitting an equivalent circuit containing a series of R-CPE-elements to the impedance spectra. These elements are intended to represent the charge transfer reaction, the interphase, and other (often unknown) processes [12,45]. The matter is further complicated by the porous structure of the graphite electrode which necessitates complex transmission lines for physics based modelling [42,46]. In this study, EIS data analysis can be significantly simplified due to the formation of a homogeneous interphase on the non-porous model anode. As discussed in a previous study [27], the SEI slows down Li-ions diffusing from the bulk electrolyte to the electrode surface and can therefore be modeled by a finite length Warburg FLW element with transmissive boundary during Li intercalation. A simulation of the electrode EIS response using a physics-based model furthermore shows that the depressed semicircle visible in the Nyquist plot $\leq$1 V is formed by the charge transfer reaction in series with diffusion limitation in the interphase [27]. A similar SEI description was also derived by Single et al. from a physics based EIS model [47]. In this work the equivalent circuit model depicted in Fig. 5 is used for fitting all C anode EIS spectra recorded $\leq$ 1 V vs. Li^+/Li. Note that the double layer capacitance is modeled as a CPE element with a constant phase value set to 0.8, as measured at high potentials (Fig. 4 a). An ideal FLW element is used for modeling Li diffusion through the interphase. As seen in Fig. 4 (c) and (d), the C sensor EIS spectra are described accurately by the proposed equivalent circuit model over the whole frequency range.

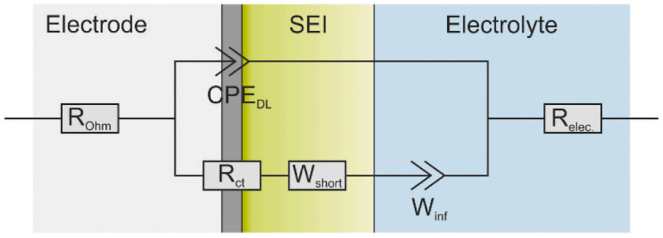

Fig. 5. Equivalent circuit model used in this work for analyzing EIS spectra recorded at $\leq$ 1 V vs. Li^+/Li on non-porous C model anodes. The interphase is modeled by a short terminus finite length Warburg element.

Fig. 6 compares the equivalent circuit fit parameters during reversible Li intercalation/insertion at low potentials in LP47, LP47 + VC, and LP47 + FEC electrolytes. Since the double layer CPE phase is the same for all EIS spectra ($CPE_{P,DL}$ = 0.8), changes in the $CPE_{T,DL}$ value are representative for changes of the C anode double layer capacitance. According to Fig. 6 (a) the C anode double layer capacitance follows the same potential dependent trends in all three tested electrolytes and decreases significantly in the first reduction cycle similar to previous observations on the copper anode current collector [27]. This phenomenon is likely related to the simultaneous formation of the SEI and could be caused by the reduction of the electrode's electroactive surface area and/or changes of the dielectric properties and charge separation at the interface. Both additives appear to slightly decrease the $CPE_{T,DL}$ during cycling. It is possible that the increased formation of inorganic salt in both VC and FEC containing electrolytes reduces the effective electroactive electrode surface area and therefore contributes to this change of electrode double layer capacitance. Since a CPE-element is used in this study for describing the electrode double layer, the precise double layer capacitance C_{DL} value remains unknown. However, one can estimate a pseudo capacitance around 0.25 V vs. Li^+/Li assuming an ideal RC-circuit with the same time constant as the R-CPE element:

$$C_{pseudo} = CPE_T^{\left(\frac{1}{CPE_P}\right)} \; R^{\left(\frac{1}{CPE_P}-1\right)} \approx 4\ \mu F\ \ cm^{-2} \tag{4}$$

Of course C_{pseudo} is only a very rough estimation of the real double layer capacitance in the cell, but it is in the realm of expected values for a Li-ion cell anode in contact with a battery electrolyte [27].

The charge transfer resistance is strongly affected by the electrode potential in the region $\leq$ 1 V vs. Li^+/Li (Fig. 6 b). In this regime different sites in the C bulk active material become available for reversible Li-ion intercalation/insertion with decreasing potential. It is possible that the rate constant of these charge transfer reactions and/or the number of

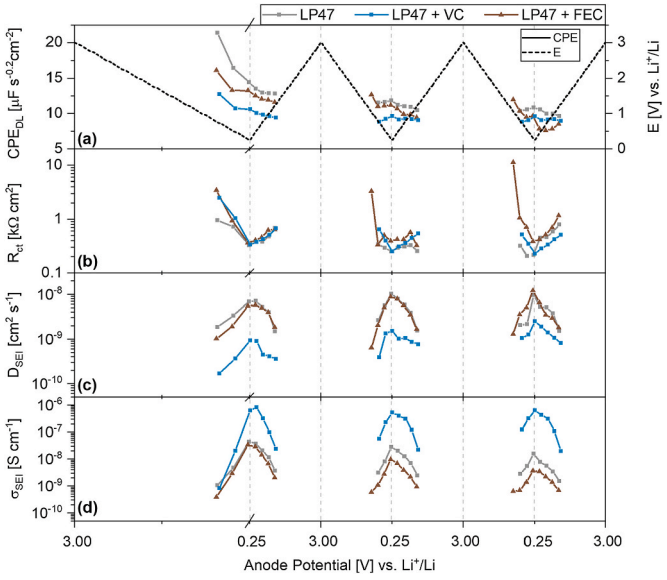

Fig. 6. Equivalent circuit parameters according to Fig. 5 fitted to EIS spectra recorded on the carbon coated QCM anode at low potentials during Li intercalation in LP47, LP47 + 0.1 wt% VC, and LP47 + 0.1 wt% FEC electrolyte. The corresponding electrochemical and interphase formation data is presented in Fig. 2. The interphase is modeled by an ideal FLW element with transmissive boundary condition.

sites accepting lithium increases with low potentials which would lower the overall R_{ct} value correspondingly. Changes in Li-ion concentration/coverage at the anode interface might also shift R_{ct} as a function of electrode potential during cycling [27]. Between cycles R_{ct} is generally becoming lower. It is possible that the interphase forming over time aids charge transfer e.g. by lowering the energy required for stripping the solvation shell off the Li-ions, as already hypothesized based on the EIS spectra plotted in Fig. 4 (b). The anode charge transfer resistance during Li insertion shown in Fig. 6 (b) is not significantly affected by introducing small amounts of VC or FEC to the cell. At 250 mV vs. Li^+/Li R_{ct} is in the range of 300 Ω cm^2 in all three tested electrolytes. The small differences are most likely within the margin of error for this experiment.

The Warburg parameters $W_{S,R}$ and $W_{S,T}$ describe mass transport through the SEI and decrease/increase with electrode potential in all three tested electrolytes (Fig. S7) as previously observed at the copper/LP47 interface [27]. In general, the values measured for Warburg resistance and time constant on C anodes in contact with additive free LP47 electrolyte are much higher compared to the Warburg parameters obtained previously for a similar system on copper anode current collectors ($W_{s,R,C} \approx 500$ Ω cm [2], $W_{s,R,Cu} \approx 7$ Ω cm [2], $W_{s,T,C} \approx 6$ ms, $W_{s,T,Cu} \approx 0.1$ ms) [27]. This indicates that Li-ion transport through the interphase is considerably slower on C anodes even though the interphase on Cu is significantly thicker ($t_{SEI,C}$ ~85 nm, $t_{SEI,Cu}$ ~ 120 nm) [27].

Several parameters, including the SEI thickness, influence the Warburg time constant and resistance. In order to investigate and compare the effect of VC and FEC on the intrinsic electrochemical interphase properties it is therefore helpful to calculate the effective SEI diffusion coefficient and conductivity by combining the results from EIS and EQCM-D according to the following equations for finite length diffusion [27]:

$$D_{SEI} = \frac{t_{SEI}^2}{W_{s,T}} \tag{5}$$

$$\sigma_{SEI} = \frac{t_{SEI}}{A \cdot W_{s,\ R}} \tag{6}$$

The diffusion coefficient of charged species traveling through the SEI plotted in Fig. 6 (c) is two to four orders of magnitude below electrolyte bulk values ($D_{electrolyte} \sim 10^{-6}$ cm^2 s^{-1}) [48,49] in all three tested electrolytes which is in accordance with the suggested equivalent circuit model [27]. As already seen from the interphase formed on copper [27] and as indicated by the reversible changes of $W_{s,R}$ and $W_{s,T}$, the SEI ion diffusion coefficient and the SEI conductivity significantly increase with decreasing anode potential during Li intercalation. It is likely that this reversible change of the interphase transport properties is related to the simultaneously detected fluctuations of the SEI viscoelastic properties shown in Fig. 2 (c) & (d). The reversible insertion of Li into the carbon active material and corresponding fluctuations of the interphase solvent fraction and the coordinated and uncoordinated EC concentration at the anode might cause this phenomenon. The SEI Li-ion diffusion coefficient at low potentials is slightly increasing between cycles in all cells, which could be correlated with the slow continuous growth of SEI viscosity observed in Fig. 2 (d) over time. Interestingly, the SEI conductivity follows a reverse trend and actually drops in blank LP47 from ~$4 \cdot 10^{-8}$ S cm^{-1} in the first cycle to ~$2 \cdot 10^{-8}$ S cm^{-1} in the third cycle at 0.25 V ($\sigma_{Electrolyte}$ ~10^{-2} S cm^{-1}) [50]. A similar trend can be observed for the cells containing electrolyte with FEC or (to a lesser extent) also VC (Fig. 6 d). One possible reason could be that ongoing interphase formation processes, triggered for example by the instability or solubility of certain SEI components and/or the reduction of water, could reduce the ion conductive fraction of the interphase (e.g. by increased formation of inorganic species such as Li_2CO_3 or LiF) [32] which in turn would reduce the effective SEI conductivity. Combined with the continuous increase of SEI thickness (Fig. 2 b) - which means that there is less dissolution of SEI components, if any, compared to the rate of SEI growth - this causes a considerable growth of the actual SEI resistance at low frequencies in the cells containing blank LP47 or LP47 + FEC electrolyte ($W_{S,R}$, see Fig. S7).

While FEC does not appear to significantly influence the effective ion diffusion coefficient in the SEI, combined EIS & EQCM-D reveals a decrease of D_{SEI} if VC is part of the initial electrolyte (Fig. 6 c). If we assume that ion conduction in the SEI occurs mainly through the organic polymer-solvent network and its pores, this could indicate that the polymeric FEC decomposition products feature similar Li-ion transport properties compared to the solid EC reduction products. The organic interphase generated by the polymerization of VC on the other hand appears to slow Li-ion diffusion considerably more. This phenomenon could possibly be related to additional cross linking in the polymeric structure expected from the catalytic radical polymerization process of VC [8,32] or also by the formation of additional poorly conductive VC decomposition products such as HCO_2Li, $Li_2C_2O_4$, or Li_2CO_3 [19].

Unlike D_{SEI} the SEI conductivity σ_{SEI} increases significantly if small quantities of VC are added to the electrolyte. Several reasons could cause these inverse trends between diffusion coefficient and conductivity such as changes of the Li-ion transference number or salt activity for example. However, EQCM-D and OEMS measurements furthermore indicate that the interphase formed by VC successfully suppresses ongoing side reactions such as the reduction of water. This in turn likely results in reduced formation of poorly conductive SEI components such as Li_2CO_3 which contributes to both the reduced interphase mass and the improved SEI conductivity. FEC on the other hand is known to generate significant amounts of LiF in the interphase during its reduction process which hampers ion diffusion and significantly reduces the interphase conductivity. The additive is furthermore not capable of preventing side reaction such as water reduction which causes the continuous drop of σ_{SEI} during cycling shown in Fig. 6 (d). Even though the interphase in LP47 + 0.1 wt% FEC contains ~20% less mass compared to pure LP47 after 3 cycles (Fig. 2 b) the overall electrode impedance increases therefore considerably with FEC during cycling, as evident from Fig. 4 (c) and (d).

3. Conclusion

Small amounts of VC or FEC added to the electrolyte significantly alter the interphase formation process at the C anode in a Li-ion cell. Both additives are reduced at potentials >1 V vs. Li^+/Li, suppress the subsequent reduction of EC, and slow other decomposition processes, which reduces the overall interphase mass by roughly 30% for FEC and 50% for VC after the first reduction cycle. The interphase formed in the electrolyte containing VC furthermore prevents the continuous reduction of water at low potentials and features overall superior passivation of the electrode compared to the additive-free system. The SEI formed by FEC reduction on the other hand does not prevent side reactions effectively which results in a continuous increase of both SEI mass and electrolyte viscosity during cycling. Both additives alter the interphasial composition and therefore also influence the SEI mechanical properties. The measured increase in SEI shear storage modulus compared to the blank electrolyte ($G'_{SEI,LP47} \ll G'_{SEI,LP47+VC} < G'_{SEI,LP47+FEC}$) is likely caused by the precipitation of compact crosslinked polymeric compounds (e.g. poly(VC)) and rigid inorganic species such as Li_2CO_3 and, in the case of FEC, also LiF at the anode interface. The SEI slows down diffusion between the electrolyte and the anode interface and can therefore be modeled as a short FLW element using impedance spectroscopy. The corresponding ion diffusion coefficient in the SEI is 2–4 orders of magnitude below the electrolyte bulk values depending on the electrolyte composition and operating potential. Small amounts of VC added to the electrolyte increase the SEI conductivity which, combined with the reduction of interphase thickness, causes a reduction of the overall anode impedance during Li intercalation. FEC on the other hand lowers the interphase conductivity and therefore increases the

impedance of the carbon electrode significantly. Both the SEI mechanical and transport properties are affected strongly by the anode operating electrochemical potential. In general, the interphase is becoming more rigid and at the same time more conductive with decreasing potential, which could be related to the reversible insertion of Li into the active material and corresponding fluctuations of the coordinated and uncoordinated EC concentration at the anode interface. Further investigations are required for a fundamental understanding of these processes and their influence on battery cell cycling.

Author contributions

Experiments and data analysis were conducted by P.G.K. The manuscript was written through contributions of all authors. All authors have given approval to the final version of the manuscript.

CRediT authorship contribution statement

Paul G. Kitz: Methodology, Software, Formal analysis, Investigation, Writing - original draft. **Matthew J. Lacey:** Formal analysis, Writing - review & editing. **Petr Novák:** Supervision, Writing - review & editing. **Erik J. Berg:** Supervision, Funding acquisition, Conceptualization, Writing - review & editing.

Declaration of competing interest

The authors declare that they have no known competing financial interests or personal relationships that could have appeared to influence the work reported in this paper.

Acknowledgment

The authors acknowledge the Swiss National Science Foundation (SNSF) under the “Ambizione Energy” funding scheme (Grant 160540) and the Knut and Alice Wallenberg (KAW) Foundation (Grant 2017.0204). We thank Christoph Bolli for assistance with the OEMS measurements and Michael Horisberger and Christine Klauser for support with electrode sputtering.

Appendix A. Supplementary data

Supplementary data to this article can be found online at https://doi.org/10.1016/j.jpowsour.2020.228567.

References

[1] J. Vetter, P. Novák, M.R. Wagner, C. Veit, K.-C. Möller, J.O. Besenhard, M. Winter, M. Wohlfahrt-Mehrens, C. Vogler, A. Hammouche, Ageing mechanisms in lithium-ion batteries, J. Power Sources 147 (1–2) (2005) 269–281, https://doi.org/10.1016/j.jpowsour.2005.01.006.

[2] K. Xu, Electrolytes and interphases in Li-ion batteries and beyond, Chem. Rev. 114 (23) (2014) 11503–11618, https://doi.org/10.1021/cr500003w.

[3] L. Wang, A. Menakath, F. Han, Y. Wang, P.Y. Zavalij, K.J. Gaskell, O. Borodin, D. Iuga, S.P. Brown, C. Wang, et al., Identifying the components of the solid–electrolyte interphase in Li-ion batteries, Nat. Chem. 11 (September) (2019), https://doi.org/10.1038/s41557-019-0304-z.

[4] A.M. Haregewoin, A.S. Wotango, B. Hwang, Electrolyte additives for lithium ion battery electrodes: progress and perspectives, Energy Environ. Sci. 9 (1) (2016) 1955–1988, https://doi.org/10.1039/c6ee00123h.

[5] D. Aurbach, K. Gamolsky, B. Markovsky, Y. Gofer, M. Schmidt, U. Heider, On the use of vinylene carbonate (VC) as an additive to electrolyte solutions for Li-ion batteries, Electrochim. Acta 47 (9) (2002) 1423–1439, https://doi.org/10.1016/S0013-4686(01)00858-1.

[6] H. Nakai, T. Kubota, A. Kita, A. Kawashima, Investigation of the solid electrolyte interphase formed by fluoroethylene carbonate on Si electrodes, J. Electrochem. Soc. 158 (7) (2011) A798, https://doi.org/10.1149/1.3589300.

[7] S.S. Zhang, K. Xu, T.R. Jow, EIS study on the formation of solid electrolyte interface in Li-ion battery, Electrochim. Acta 51 (8–9) (2006) 1636–1640, https://doi.org/10.1016/j.electacta.2005.02.137.

[8] B. Zhang, M. Metzger, S. Solchenbach, M. Payne, S. Meini, H.A. Gasteiger, A. Garsuch, B.L. Lucht, Role of 1,3-propane sultone and vinylene carbonate in solid electrolyte interface formation and gas generation, J. Phys. Chem. C 119 (21) (2015) 11337–11348, https://doi.org/10.1021/acs.jpcc.5b00072.

[9] H. Ota, Y. Sakata, A. Inoue, S. Yamaguchi, Analysis of vinylene carbonate derived SEI layers on graphite anode, J. Electrochem. Soc. 151 (10) (2004) A1659, https://doi.org/10.1149/1.1785795.

[10] M. Nie, J. Demeaux, B.T. Young, D.R. Heskett, Y. Chen, A. Bose, J.C. Woicik, B. L. Lucht, Effect of vinylene carbonate and fluoroethylene carbonate on SEI formation on graphitic anodes in Li-ion batteries, J. Electrochem. Soc. 162 (13) (2015) A7008–A7014, https://doi.org/10.1149/2.0021513jes.

[11] J.C. Burns, R. Petibon, K.J. Nelson, N.N. Sinha, A. Kassam, B.M. Way, J.R. Dahn, Studies of the effect of varying vinylene carbonate (VC) content in lithium ion cells on cycling performance and cell impedance, J. Electrochem. Soc. 160 (10) (2013) A1668–A1674, https://doi.org/10.1149/2.031310jes.

[12] D. Pritzl, S. Solchenbach, M. Wetjen, H.A. Gasteiger, Analysis of vinylene carbonate (VC) as additive in graphite/LiNi0.5Mn1.5O4 cells, J. Electrochem. Soc. 164 (12) (2017) A2625–A2635, https://doi.org/10.1149/2.1441712jes.

[13] D.Y. Wang, N.N. Sinha, J.C. Burns, C.P. Aiken, R. Petibon, J.R. Dahn, A comparative study of vinylene carbonate and fluoroethylene carbonate additives for LiCoO2/graphite pouch cells, J. Electrochem. Soc. 161 (4) (2014) A467–A472, https://doi.org/10.1149/2.001404jes.

[14] L. Hu, Z. Zhang, K. Amine, Fluorinated electrolytes for Li-ion battery: an FEC-based electrolyte for high voltage LiNi0.5Mn1.5O4/graphite couple, Electrochem. Commun. 35 (2013) 76–79, https://doi.org/10.1016/j.elecom.2013.08.009.

[15] Y. Li, F. Lian, L. Ma, C. Liu, L. Yang, X. Sun, K. Chou, Fluoroethylene carbonate as electrolyte additive for improving the electrochemical performances of high-capacity Li1.16[Mn0.75Ni0.25]0, 84O2 Material. *Electrochim. Acta* 168 (2015) 261–270, https://doi.org/10.1016/j.electacta.2015.04.030.

[16] R. Jung, M. Metzger, D. Haering, S. Solchenbach, C. Marino, N. Tsiouvaras, C. Stinner, H.A. Gasteiger, Consumption of fluoroethylene carbonate (FEC) on Si-C composite electrodes for Li-ion batteries, J. Electrochem. Soc. 163 (8) (2016) A1705–A1716, https://doi.org/10.1149/2.0951608jes.

[17] R. Petibon, V.L. Chevrier, C.P. Aiken, D.S. Hall, S.R. Hyatt, R. Shunmugasundaram, J.R. Dahn, Studies of the capacity fade mechanisms of LiCoO $_2$/Si-alloy: graphite cells, J. Electrochem. Soc. 163 (7) (2016) A1146–A1156, https://doi.org/10.1149/2.0191607jes.

[18] R. McMillan, H. Slegr, Z.X. Shu, W. Wang, Fluoroethylene carbonate electrolyte and its use in lithium ion batteries with graphite anodes, J. Power Sources 81–82 (1999) 20–26, https://doi.org/10.1016/S0378-7753(98)00201-8.

[19] A.L. Michan, B.S. Parimalam, M. Leskes, R.N. Kerber, T. Yoon, C.P. Grey, B. L. Lucht, Fluoroethylene carbonate and vinylene carbonate reduction: understanding lithium-ion battery electrolyte additives and solid electrolyte interphase formation, Chem. Mater. 28 (22) (2016) 8149–8159, https://doi.org/10.1021/acs.chemmater.6b02282.

[20] K.U. Schwenke, S. Solchenbach, J. Demeaux, B.L. Lucht, H.A. Gasteiger, The impact of CO2 evolved from VC and FEC during formation of graphite anodes in lithium-ion batteries, J. Electrochem. Soc. 166 (10) (2019) A2035–A2047, https://doi.org/10.1149/2.0821910jes.

[21] P.G. Kitz, P. Novák, E.J. Berg, Influence of water contamination on the SEI formation in Li-ion cells: an operando EQCM-D study, ACS Appl. Mater. Interfaces 12 (13) (2020) 15934–15942, https://doi.org/10.1021/acsami.0c01642.

[22] Y. Ein-Eli, B. Markovsky, D. Aurbach, Y. Carmeli, H. Yamin, S. Luski, The dependence of the performance of Li-C intercalation anodes for Li-ion secondary batteries on the electrolyte solution composition, Electrochim. Acta 39 (17) (1994) 2559–2569, https://doi.org/10.1016/0013-4686(94)00221-5.

[23] S. Grugeon, P. Jankowski, D. Cailleu, C. Forestier, L. Sannier, M. Armand, P. Johansson, S. Laruelle, Towards a better understanding of vinylene carbonate derived SEI-layers by synthesis of reduction compounds, J. Power Sources 427 (February) (2019) 77–84, https://doi.org/10.1016/j.jpowsour.2019.04.061.

[24] C. Xu, F. Lindgren, B. Philippe, M. Gorgoi, F. Björefors, K. Edström, T. Gustafsson, Improved performance of the silicon anode for Li-ion batteries: understanding the surface modification mechanism of fluoroethylene carbonate as an effective electrolyte additive, Chem. Mater. 27 (7) (2015) 2591–2599, https://doi.org/10.1021/acs.chemmater.5b00339.

[25] I.A. Shkrob, J.F. Wishart, D.P. Abraham, What makes fluoroethylene carbonate different? J. Phys. Chem. C 119 (27) (2015) 14954–14964, https://doi.org/10.1021/acs.jpcc.5b03591.

[26] K. Leung, S.B. Rempe, M.E. Foster, Y. Ma, J.M. Martinez del la Hoz, N. Sai, P. B. Balbuena, Modeling electrochemical decomposition of fluoroethylene carbonate on silicon anode surfaces in lithium ion batteries, J. Electrochem. Soc. 161 (3) (2014) A213–A221, https://doi.org/10.1149/2.092401jes.

[27] P.G. Kitz, M.J. Lacey, P. Novák, E.J. Berg, Operando EQCM-D with simultaneous in situ EIS: new insights into interphase formation in Li ion batteries, Anal. Chem. 91 (3) (2019) 2296–2303, https://doi.org/10.1021/acs.analchem.8b04924.

[28] M. He, E. Castel, A. Laumann, G. Nuspl, P. Novák, E. Berg, J. In situ gas analysis of Li4Ti5O12 based electrodes at elevated temperatures, J. Electrochem. Soc. 162 (6) (2015) A870–A876, https://doi.org/10.1149/2.0311506jes.

[29] IAM - Karlsruhe Institute of Technology, Lin-KK tool, http://www.iwe.kit.edu/Lin-KK.php. accessed May 1, 2018.

[30] K. Kwon, F. Kong, F. McLarnon, J.W. Evans, Characterization of the SEI on a carbon film electrode by combined EQCM and spectroscopic ellipsometry, J. Electrochem. Soc. 150 (2) (2003) A229, https://doi.org/10.1149/1.1538223.

[31] M. Metzger, B. Strehle, S. Solchenbach, H.A. Gasteiger, Hydrolysis of ethylene carbonate with water and hydroxide under battery operating conditions, J. Electrochem. Soc. 163 (7) (2016) A1219–A1225, https://doi.org/10.1149/2.0411607jes.

[32] S.K. Heiskanen, J. Kim, B.L. Lucht, Generation and evolution of the solid electrolyte interphase of lithium-ion batteries, Joule 3 (10) (2019) 2322–2333, https://doi.org/10.1016/j.joule.2019.08.018.
[33] S.K. Jeong, M. Inaba, R. Mogi, Y. Iriyama, T. Abe, Z. Ogumi, Surface film formation on a graphite negative electrode in lithium-ion batteries: atomic force microscopy study on the effects of film-forming additives in propylene carbonate solutions, Langmuir 17 (26) (2001) 8281–8286, https://doi.org/10.1021/la015553h.
[34] M.E. Spahr, T. Palladino, H. Wilhelm, A. Würsig, D. Goers, H. Buqa, M. Holzapfel, P. Novák, Exfoliation of graphite during electrochemical lithium insertion in ethylene carbonate-containing electrolytes, J. Electrochem. Soc. 151 (9) (2004) A1383, https://doi.org/10.1149/1.1775224.
[35] C. Xu, G. Hernández, S. Abbrent, L. Kobera, R. Konefal, J. Brus, K. Edström, D. Brandell, J. Mindemark, Unraveling and mitigating the storage instability of fluoroethylene carbonate-containing LiPF6 electrolytes to stabilize lithium metal anodes for high-temperature rechargeable batteries, ACS Appl. Energy Mater. 2 (7) (2019) 4925–4935, https://doi.org/10.1021/acsaem.9b00607.
[36] K. Kim, I. Park, S.Y. Ha, Y. Kim, M.H. Woo, M.H. Jeong, W.C. Shin, M. Ue, S. Y. Hong, N.S. Choi, Understanding the thermal instability of fluoroethylene carbonate in LiPF6-based electrolytes for lithium ion batteries, Electrochim. Acta 225 (2017) 358–368, https://doi.org/10.1016/j.electacta.2016.12.126.
[37] D. Strmcnik, I.E. Castelli, J.G. Connell, D. Haering, M. Zorko, P. Martins, P. P. Lopes, B. Genorio, T. Østergaard, H.A. Gasteiger, et al., Electrocatalytic transformation of HF impurity to H2 and LiF in lithium-ion batteries, Nat. Catal. 1 (4) (2018) 255–262, https://doi.org/10.1038/s41929-018-0047-z.
[38] O. Matsuoka, A. Hiwara, T. Omi, M. Toriida, T. Hayashi, C. Tanaka, Y. Saito, T. Ishida, H. Tan, S.S. Ono, et al., Ultra-thin passivating film induced by vinylene carbonate on highly oriented pyrolytic graphite negative electrode in lithium-ion cell, J. Power Sources 108 (1–2) (2002) 128–138, https://doi.org/10.1016/S0378-7753(02)00012-5.
[39] C.C. Nguyen, B.L. Lucht, Comparative study of fluoroethylene carbonate and vinylene carbonate for silicon anodes in lithium ion batteries, J. Electrochem. Soc. 161 (12) (2014) A1933–A1938, https://doi.org/10.1149/2.0731412jes.
[40] I. Yoon, S. Jurng, D.P. Abraham, B.L. Lucht, P.R. Guduru, Measurement of mechanical and fracture properties of solid electrolyte interphase on lithium metal anodes in lithium ion batteries, Energy Stor. Mater. (October) (2019), https://doi.org/10.1016/j.ensm.2019.10.009.
[41] Z. Yang, M.C. Dixon, R.A. Erck, L. Trahey, Quantification of the mass and viscoelasticity of interfacial films on tin anodes using EQCM-D, ACS Appl. Mater. Interfaces 7 (48) (2015) 26585–26594, https://doi.org/10.1021/acsami.5b07966.
[42] D. Pritzl, J. Landesfeind, S. Solchenbach, H.A. Gasteiger, An analysis protocol for three-electrode Li-ion battery impedance spectra: Part II. Analysis of a graphite anode cycled vs, LNMO. *J. Electrochem. Soc.* 165 (10) (2018) A2145–A2153, https://doi.org/10.1149/2.0461810jes.
[43] J.B. Jorcin, M.E. Orazem, N. Pébère, B. Tribollet, CPE analysis by local electrochemical impedance spectroscopy, Electrochim. Acta 51 (8–9) (2006) 1473–1479, https://doi.org/10.1016/j.electacta.2005.02.128.
[44] D.P. Abraham, M.M. Furczon, S.H. Kang, D.W. Dees, A.N. Jansen, Effect of electrolyte composition on initial cycling and impedance characteristics of lithium-ion cells, J. Power Sources 180 (1) (2008) 612–620, https://doi.org/10.1016/j.jpowsour.2008.02.047.
[45] D. Juarez-Robles, C. Chen, Y. Barsukov, P.P. Mukherjee, Impedance evolution characteristics in lithium-ion batteries, J. Electrochem. Soc. 164 (4) (2017) A837–A847, https://doi.org/10.1149/2.1251704jes.
[46] N. Ogihara, Y. Itou, T. Sasaki, Y. Takeuchi, Impedance spectroscopy characterization of porous electrodes under different electrode thickness using a symmetric cell for high-performance lithium-ion batteries, J. Phys. Chem. C 119 (9) (2015) 4612–4619, https://doi.org/10.1021/jp512564f.
[47] F. Single, B. Horstmann, A. Latz, Theory of impedance spectroscopy for lithium batteries, J. Phys. Chem. C 123 (2019) 27327–27343, https://doi.org/10.1021/acs.jpcc.9b07389.
[48] L.O. Valoen, J.N. Reimers, Transport properties of LiPF6-based Li-ion battery electrolytes, J. Electrochem. Soc. 152 (5) (2005) A882, https://doi.org/10.1149/1.1872737.
[49] C. Capiglia, Y. Saito, H. Kageyama, P. Mustarelli, T. Iwamoto, T. Tabuchi, H. Tukamoto, 7Li and 19F diffusion coefficients and thermal properties of non-aqueous electrolyte solutions for rechargeable lithium batteries, J. Power Sources 81–82 (1999) 859–862, https://doi.org/10.1016/S0378-7753(98)00237-7.
[50] E.R. Logan, E.M. Tonita, K.L. Gering, J. Li, X. Ma, L.Y. Beaulieu, J.R. Dahn, A study of the physical properties of Li-ion battery electrolytes containing esters, J. Electrochem. Soc. 165 (2) (2018) A21–A30, https://doi.org/10.1149/2.0271802jes.